Articles

Molecular Modeling of *p*-Chlorophenoxyacetic Acid Binding to the CLC-0 Channel†

Oscar Moran,* Sonia Traverso, Laura Elia, and Michael Pusch

Istituto di Biofisica, Sezione di Genova, CNR, Via De Marini, 6, I-16149 Genova, Italy

Received December 17, 2002; Revised Manuscript Received March 21, 2003

ABSTRACT: Molecular simulation techniques were applied to predict the interaction of the CLC-0 Cl^- channel and the channel-blocking molecule *p*-chlorophenoxyacetic acid (CPA). A three-dimensional model of the CLC-0 channel was constructed on the basis of the homology with the bacterial Cl^- channel StCLC, the structure of which has been solved by X-ray crystallography. Docking of the CPA molecule was obtained by using a geometric recognition algorithm, yielding 5000 possible conformations. By restraining the simulation to those conformations in which CPA is near the intracellular mouth of the channel, the CPA−protein complex models were reduced to three sets of conformations, which are interconvertible within 2 ns when molecular dynamics is applied to the system. Point mutations of CLC-0 at three different positions predicted to interact with CPA in these configurations did, however, not greatly alter CPA inhibition, suggesting a deeper final binding location. In the model, binding of CPA to a more internal position in the ionic pathway was obtained by applying a constant force vector to CPA, pushing it toward the center of the channel. This technique allowed us to outline the possible intrachannel pathway of CPA and to describe qualitatively the binding sites and energy barriers of this pathway. The consistency of the obtained models and the experimental data indicates that the CLC-0−CPA complex model is reasonable and can be used in further biological studies, such as rational design of blocking agents of and mutagenesis of CLC Cl^- channels.

The Cl^- channel from the electric ray, CLC-0, represents the prototype of the CLC Cl^- channel family, the members of which are widely distributed in vertebrates and are involved in various inherited disorders in humans (*1*). Recently, the three-dimensional (3D) structure of bacterial CLC homologues was resolved at 3-Å resolution (*2*), providing an important basis for a mechanistic investigation of the functional mechanisms of these channels. For the well-studied class of voltage-gated cation channels, small substances that interact with the pore have been important tools for studying gating and permeation (*3*). High-affinity ligands are lacking for CLC channels, but recently, derivatives of clofibric acid have been shown to be moderately efficient blockers of CLC-0 and CLC-1, the muscle Cl^- channel (*4*−*9*). The first compound of this family that has been found to be effective on Cl^- channels is *p*-chlorophenoxypropionic acid (CPP), which inhibits the macroscopic skeletal muscle Cl^- conductance in a stereospecific manner, with the (*S*)-(−)-enantiomer being much more potent than the (*R*)-(+)-enantiomer (*10*). Work on the heterologously expressed CLC channels revealed that these substances act from the intracellular side in a strongly voltage-dependent manner. The voltage dependence arises mostly from the fact that clofibric acid binds preferentially to closed channels, while the open-channel affinity is very small (*5*).

Although the affinity of these small organic compounds is several orders of magnitude smaller than that observed for high-affinity blocking toxins in other channels, these compounds constitute promising lead compounds in the search for more specific Cl^- channels blockers. Design of more specific and potent Cl^- channel blockers has been prevented by the lack of a plausible hypothesis of the molecular structure of CLC channels. It was known that CLC channels have an unusual architecture with a dimeric structure in which each subunit forms a proper pore (*11*−*14*). The successful crystallization and X-ray diffraction of bacterial channels, which are homologous to the vertebrate CLC family (*2*), has revealed that CLC channels have an amazingly complex fold, with 18 α-helices per subunit. Only some of these helixes fully traverse the membrane, and most are severely tilted with respect to an orientation perpendicular to the membrane surface.

The availability of the 3D structure opened the possibility to construct models of members of the CLC family polypeptides. We have undertaken homology modeling of CLC-0, and we have studied the docking of the simplest clofibric acid derivative, *p*-chlorophenoxyacetic acid (CPA),[1] to the intracellular mouth of the ionic pore of the channel. We have

† This work has been partially supported by grants from Telethon Italy (project 1079) and MIUR Italy (FIRB RBAU01PJMS) to M.P.

* To whom correspondence should be addressed. Fax: +39-0106475500. E-mail: moran@ge.cnr.it.

10.1021/bi027368o CCC: $25.00
Published on Web 04/16/2003

found that CPA has an apparent favorable binding site at the intracellular entrance of the channel. However, when pushed by a mechanic force, this molecule can penetrate along the channel pore, to reach a position close to a highly conserved glutamic acid residue that has been proposed to play a key role in gating (*2*).

METHODS

Homology Modeling. Homology modeling was done by fitting the primary sequence of the *Torpedo marmorata* Cl^- channel polypeptide (GenBank number X56758) to the 3D structure of the *Salmonella typhymurium* (StCLC, PDB accession code 1KPL) that has been recently solved by X-ray crystallography at 3-Å resolution (*2*). Structural fitting was done using Swiss-Model (www.expasy.ch/swissmod/), which is a homology modeling server Web interface (*15*−*17*). Further refinements, including the search for side-chain rotamers, reconstruction of loops, and preliminary energy minimization, were done using Swiss-PdbViewer (SPDBV) (*15*). Further minimization was done with NAMD2 (*18*), using the Amber99 force field (*19*). Force field parameters for CPA were estimated using the module ANTECHAMBER of AMBER 7 (*20*). The evaluation of structural parameters and prediction quality of the modeled structure was done using the programs WHATIF (*21*, *22*) from the Biotech Web server (biotech.embl-ebi.ac.uk).

Protein Docking. The geometry of the *p*-chlorophenoxyacetic acid (CPA) molecule was adjusted with the UFF method (*23*), using the commercial program ArgusLab (Planaria Software). To predict the structure of the channel−toxin complex, we applied a geometric recognition algorithm, implemented in the program GRAMM (*24*). The program performs an exhaustive six-dimensional search through the relative translations and rotations of the molecules. The prediction was done with parameters designed for high-resolution structures (*24*), and the 5000 lowest energy configurations were analyzed.

Molecular Dynamics. For molecular dynamics (MD), we constructed a complex system, including a phospholipid bilayer and a shell of water. The baricenter of the CLC-0 model, including the docked ligand, was located in the center of crystalline dimiristoyl-phosphatidylcholine (DMP) (*25*), and the phospholipid molecules in contact with the protein were extruded. To simulate explicitly the solvent, the system, except for the borders of the lipid bilayer, were hydrated with a shell of TIP3P water model (*26*) using the LEAP module of AMBER 7 (*20*). The complete model included also a Cl^- inside each channel subunit, similar to that found in the StCLC (*2*). The system was limited to phospholipid and water molecules at a distance of 18 Å from the protein, to reduce the number of elements used in the simulations (see Figure 2E).

All MD simulations presented in this work were done with the NAMD2 program, using the Amber99 force field. All the simulations were carried out at 300 K. The SHAKE (*27*) procedure was employed to constrain all bonds connecting hydrogen atoms. The time step of the simulations was 2 fs, with a cutoff at 12 Å for the nonbonded interactions. The nonbonded pairs were updated every 20 steps. All atoms within 13 Å of the CLC-0 were allowed to move. Atoms between 13 and 18 Å were restrained by a 20 kcal mol^{-1} $Å^{-2}$ harmonic force.

Prior to MD simulations, a series of minimizations were carried out with each complex model, with a maximum number of steps of 50 000. A convergence criterion for the energy gradient of 0.5 kcal mol^{-1} $Å^{-1}$ was attained in all cases. After minimization, CPA−CLC-0 complexes were stepwise heated to 300 K and equilibrated for at least 200 ps at the final temperature. Data collection was then carried out for 0.5−3 ns.

To "force" the CPA to reach a putative binding site in a more internal position in the channel, a constant force was applied to the CPA molecule in a series of MD simulations. When forced MD was used, one CPA molecule was localized near each subunit, in a random position, 2 ± 1 Å from the baricenter of the residues R305, R312, P522, and F526, which demarcate the intracellular entrance of the channel. After minimization and equilibration, a constant force vector of 69−483 fN (0.1−0.7 kcal mol^{-1} $Å^{-1}$) was applied to all CPA atoms. The vector was defined to "push" the CPA molecule from its initial baricenter toward the residue E166 of the corresponding subunit, which is hypothesized to form part of the channel-gating machinery (*2*). We evaluated the trajectory of CPA on the same axis of the applied force by measuring the time of permanency of the ligand at a given position on each simulation. To construct the overall histogram of probability of CPA to occupy a position along the reference axis, the probability distributions measured for each experiment were accumulated in a weighted sum, such that the biased potentials due to the applied force were discounted. The weights were calculated by the weighed histogram analysis method (WHAM) (*28*). Close interactions and hydrogen bonding between CPA and the CLC-0 model were determined by the programs LIGPLOT and HHBOND, respectively (*29*, *30*).

Molecular Biology and Current Recording. Mutations R305Q, R305E, R312Q, and P522S were introduced into CLC-0, containing the mutation C212S by standard recombinant PCR mutagenesis. The mutation C212S has been shown to eliminate most of the slow gating process (*31*). All constructs were cloned into the PTLN vector (*7*). The final constructs were verified by sequencing over the PCR-generated fragments. cRNAs were synthesized from cDNAs after linearization with *Mlu*I, using the SP6 mMessage mMachine kit (Ambion, Austin, TX).

Xenopus oocytes were injected with 50 nL of the cRNA and incubated at 18 °C for 2−5 days. Currents were measured using the inside-out configuration of the patch clamp technique (*32*), with an EPC-7 (List, Darmstadt, Germany) amplifier and the acquisition program Pulse (HEKA, Lambrecht/Pfalz, Germany) as described previously (*6*).

The bath (internal) solution contained 100 mM *N*-methyl-D-glucamine (NMDG)-Cl, 2 mM $MgCl_2$, 10 mM HEPES, 2 mM EGTA, pH 7.3, while the standard extracellular (pipet) solution contained 100 mM NMDG-Cl, 5 mM $MgCl_2$, 10 mM HEPES, pH 7.3. CPA was applied to the internal side of the membrane by inserting the patch pipet into perfusion tubes of about 0.5-mm diameter.

[1] Abbreviations: CPA, *p*-chlorophenoxyacetic acid; DMP, dimiristoyl-phosphatidylcholine; NMDG, *N*-methyl-D-glucamine; HEPES, 4-(2-hydroxyethyl)-1-piperazineethanesulfonic acid; EGTA, ethylene glycol-bis(aminoethyl ether)-*N*′,*N*′,*N*′,*N*′-tetraacetic acid.

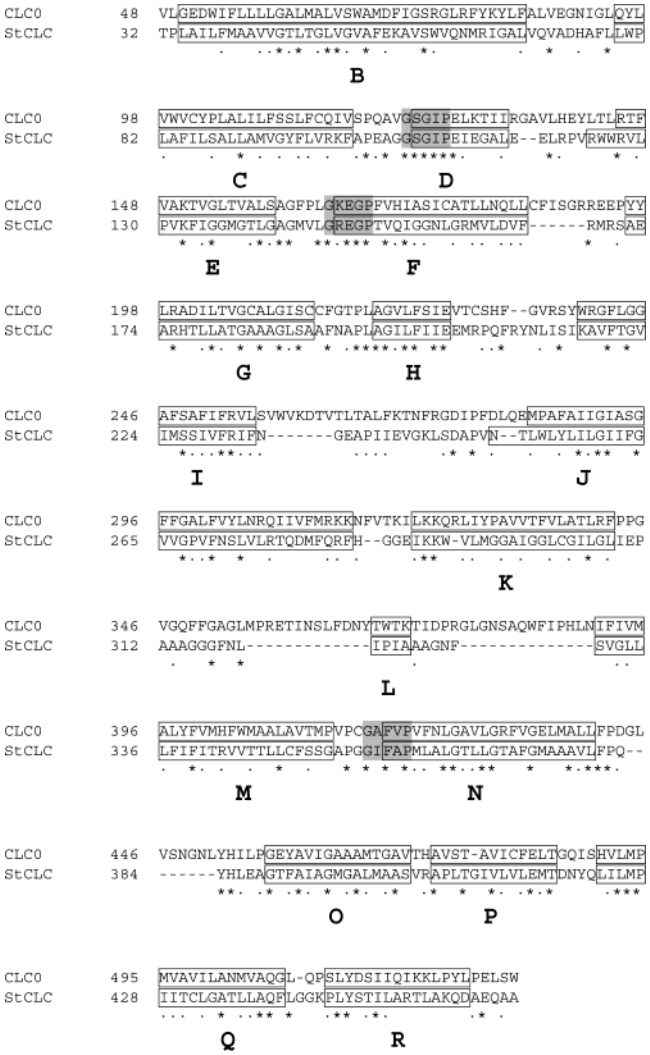

FIGURE 1: Alignment of the primary structure of the CLC-0 and StCLC polypeptides. Identical residues are indicated by asterisks, and conservative substitutions are indicated by dots. The 17 helixes of the StCLC structure, named B to R, and the corresponding homologous regions in the CLC-0 sequence are shown in boxes. Gray background identifies the conserved selectivity filter residues.

RESULTS

CLC-0 Model. The coordinates reported for the StCLC were used as template for the structural prediction of CLC-0. In Figure 1, we show the alignment of the amino acid sequences of CLC-0 and StCLC. Residues presented in the alignment are those included in the PDB file for StCLC and the corresponding residues for CLC-0. In both cases, a small segment of the N-terminus (31 and 47 residues for StCLC and CLC-0, respectively) was ignored. In the C-terminus, a small segment of 10 residues of StCLC was not included, while a longer segment of 309 residues of CLC-0, putatively intracellular, was ignored. The two polypeptide sequences shown in Figure 1 have 45% similarity, including 22% identical residues. Secondary structure prediction is very similar for the two sequences, as expected from the high similarity score.

Most of the CLC-0 model could be constructed by homology to StCLC, and it resulted in 17 helixes, named **B** to **R** (*2*) and indicated with boxes in Figure 1. Figure 2 shows a cartoon representation of the two subunits (colored in light blue and light green) of the StCLC template (Figure 2A,C)

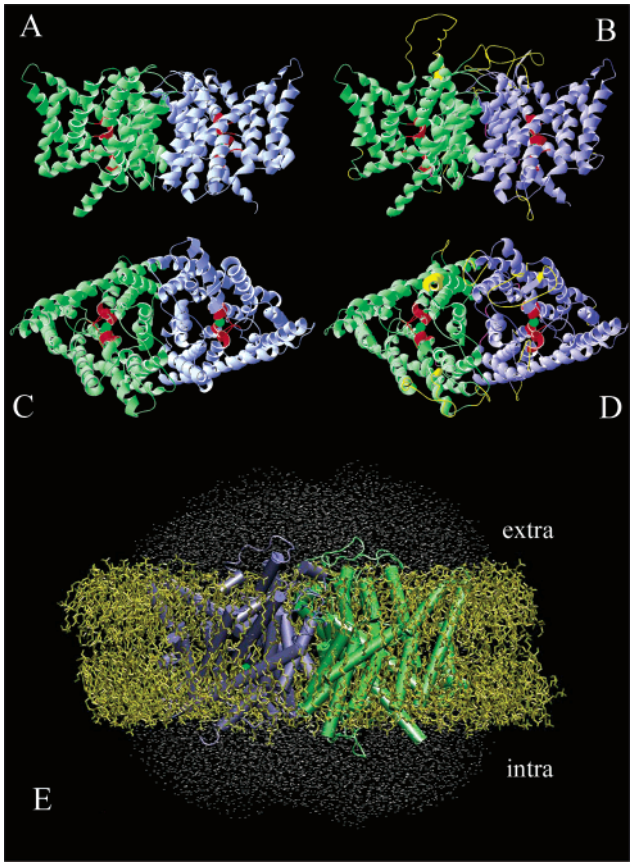

FIGURE 2: Modeling of the CLC-0 channel. Compare the cartoon drawn for the experimental 3D structure of the StCLC (A and C) and of the modeled CLC-0 (B and D) dimers. The Cl^- is represented as green spheres. The selectivity filter region is colored in red. Both structures, experimental and modeled, have 17 helixes distributed very similarly. The reconstructed loops of CLC-0 are indicated in yellow. (E) The CLC-0 model is immersed in a DMP bilayer (yellow), and the extracellular and intracellular sides of the model are hydrated with a cap of water (white dots).

and the CLC-0 model (Figure 2B,D). It is seen that the two structures have a similar packing of the α-helices of the proteins, conserving the region that putatively interacts with the Cl^- ions (green spheres) in the pores of the channel, drawn in red. As shown in Figure 1, the sequence of CLC-0 is longer than that of StCLC, in particular the loops between the helical regions. It is interesting to observe that, in the extracellular side of CLC-0, the loops are notably longer than those in the template. Obviously, these missed loops in CLC-0, shown in yellow in Figure 2, could not be modeled by homology but have been reconstructed on the basis of a loop database included in the SPDBV.

The root-mean-square deviation (RMSD) of the backbone (carboxylic carbon, α-carbon, and amino nitrogen) of CLC-0 from the StCLC template was measured along the residues included in the homology, yielding an overall RMSD of 0.116 Å, which is significantly smaller than the value of 0.5 Å predicted as the average deviation between homologous structures (*33*). To evaluate the correctness of the predicted model, a series of quality controls, using the program WHATIF, were done. Using bond angles and lengths, the position-specific rotamer distribution for every residue was determined, and the correct hydrogen bonds of the buried residues conform to the goodness criteria defined in the WHATIF program.

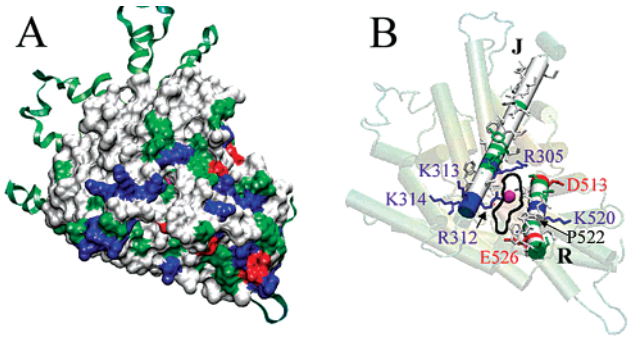

FIGURE 3: Internal surface of the CLC-0 channel model. (A) The molecular surface was calculated using the algorithm SURF (*41*), with a probe of 1.4 Å. Residues are colored by type (blue, basic; red, acidic; green, polar; and white, hydrophobic). (B) A cartoon of the channel in the same orientation as in panel A. The two helixes, **J** and **R**, forming the "lips" of the pore entry are highlighted. The Cl^- ion inside the channel is represented as a pink sphere. The contour of the border of the pore mouth is drawn for clarity.

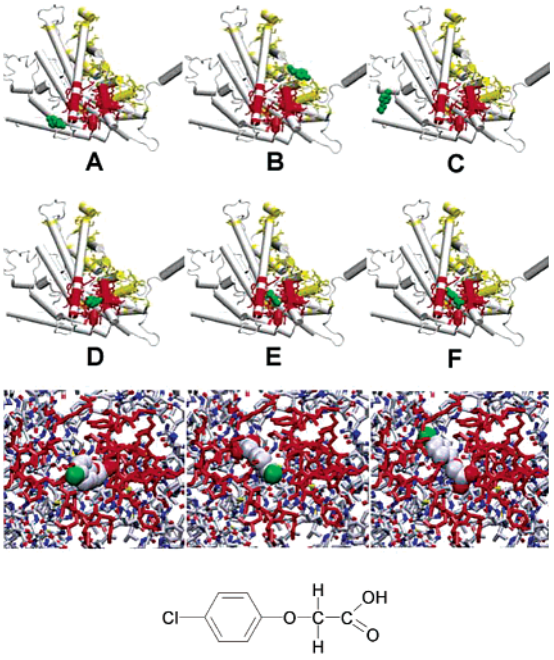

FIGURE 4: Docking models of CPA and CLC-0. The region of contact between two adjacent CLC-0 channel subunits is colored yellow, the region in the vicinity of the intracellular pore entrance is colored red, and CPA is colored green. (A−C) Incorrect models, as the ligand is bound far from the putative receptor at the entrance of the pore. (D−F) Probable correct models, as CPA is closely interacting with the pore mouth. A detailed magnification of such an interaction is shown for these three models. The CPA chlorine is colored green in the magnification. Observe, even conforming the to distance restraints, that the CPA has different orientations: in models D and E, the chlorine atom of CPA is external, while in model F it is internal. The two-dimensional structure of CPA is shown in the bottom panel.

CPA−CLC-0 Geometrical Docking. The docking simulation was done by searching the geometrical interaction of CPA with the intracellular mouth of the CLC-0 channel model shown in Figure 3A. The chemical structure of the CPA is shown in the lower panel of Figure 4. To reduce the amount of calculations, only one subunit (without any DMP or water molecules included) was used in the geometrical docking. The docking program GRAMM yielded 5000 lowest-energy possible positions for the interaction between each of the ligands and the CLC-0 used for simulation. As the calculation performs an exhaustive search for all possible low-energy configurations, without any restraints, a series of improbable configurations were also produced, as observed by visual inspection of the CLC-0−ligand complexes. For example, in some models the interaction of the ligand with the channel did not result in an evident obstruction of the pore, even if the ligand was at the intracellular surface of the channel (Figure 4A). In other models, the ligand was evidently in contact with nonexposed parts of the channel, as the region of close contact between subunits (Figure 4B) or the areas in contact with the lipid core of the membrane (see Figure 4C). Therefore, a "filter" of models was designed to select such models where the ligand is inserted in the entrance of the intracellular mouth of the channel permeation pore. The entrance of the pore is delimited by two helices, **J** and **R**, with two protruding "turrets" at the sides of the entrance. One turret is formed by the C-terminus of the helix **R** and contains an acidic residue, E526, and more deeply, in the base of the turret, the basic residue, K519, which form part of the wall of the pore. Other charged residues of helix **R**, E513 and K520, do not face toward the channel lumen. The other side of the entrance is formed by the C-terminus of the helix **J**, which is rich in basic residues, with R305 and R312 directly facing the entrance of the pore and K313 and K314 defining the basic character of the turret. The positions of these residues with respect to the pore entrance are shown in Figure 3B.

To define the interaction between the ligand and the pore, we have selected four CLC-0 residues: S123 and Y512, which correspond to S109 and Y445 in the StCLC, are very near the permeant Cl^- ion and are putatively involved in the selectivity filter (*2*). By analogy to reports for StCLC, it is expected that permeant Cl^- is partially coordinated by S123. Mutations of S123 have been demonstrated to affect channel conductance and permeability (*34*). The other two selected residues, I518 and K519 (adjacent to R451 of StCLC), have been proposed to form part of the external rim of the pore (*2*), as mutations in these regions also alter the ionic permeation of the channel (*11*, *35*). Possible correct models of the ligand−channel complex were selected with the criterion of a distance between the ligand and each of the amino acids of less than 7 Å. After the distance filter was used, the original 5000 models for each complex were greatly reduced to 15 models for the CPA−CLC-0 complex. Examples of accepted models of interaction between CPA and CLC-0 are presented in Figure 4D−F.

The structure of the StCLC channel was reported with the presence of a Cl^- channel in the intracellular side of the pore. We have not found differences when the docking procedure was applied with or without Cl^- in this position, probably because the other geometrical restraints do not allow the ligands to approach close enough to the Cl^- binding site to "perceive" the presence of the ion.

To characterize the resulting models, interatomic distances between the carboxyl carbon and the chlorine atom of the ligand and a given atom of pore-forming residues were measured. As an example, in Figure 5, we present the distances measured for CPA and CB[2] of S123, CZ of R312,

[2] Atom nomenclature for amino acids is defined according to the standard names used in the Protein Data Band (www.rcsb.org).

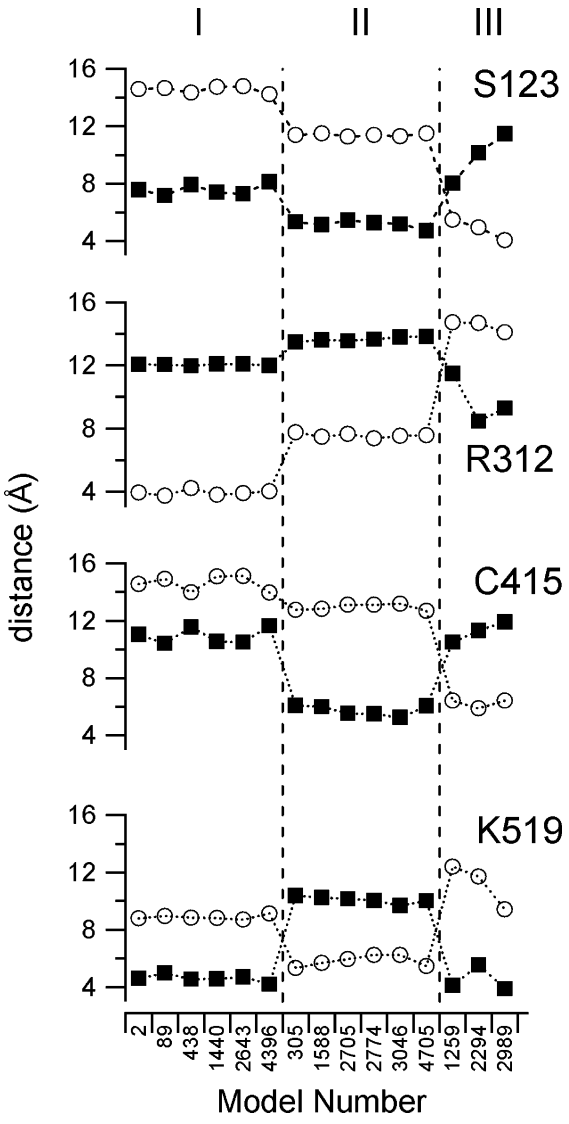

FIGURE 5: Interatomic distances between the CPA and three pore residues, measured in all accepted binding models. For each residue, the distance was measured between the carboxyl carbon (open circles) and chlorine (squares) of the CPA ligand and CB of S123, CZ of R312, SG of C415, and NZ of K519. The model number is indicated at the bottom for each set of measurements. The distances can be classified in three sets of equivalent models, indicated as I, II, and III in the figure.

SG of C415, and NZ of K519. Interatomic distances are clearly clustered in three distinguishable groups, which represent three sets of equivalent models, named I, II, and III. In sets I and II, CPA is exposed with the chlorine atom toward the cytoplasmic space and the carboxyl carbon orientated to the interior of the pore (Figure 4D,E, respectively). The difference among these two sets is that, in set I, CPA is slightly tilted in the direction of helix **R**, while in set II it is tilted toward helix **J**. A completely opposite orientation of the ligand is found in set III (Figure 4F), where the carboxylic carbon is exposed to the cytoplasmic space and the chlorine atom of CPA is situated toward in the pore.

Molecular Dynamics of Docked Ligand. The MD simulation applied to a given selected model demonstrated that the ligand position described by simple geometrical docking is only a possible conformation for the binding. Moreover, we have observed that the three described sets of conformations (I, II, and III) are interchangeable during the MD simulation.

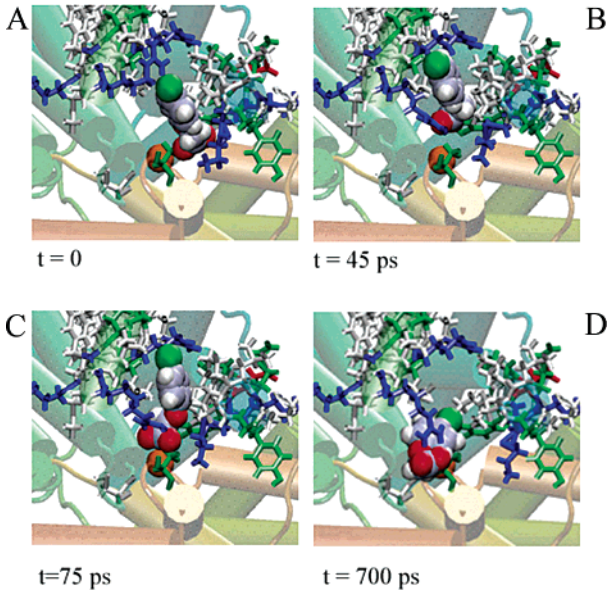

FIGURE 6: Snapshot of a MD simulation of the configuration II of the CPA−CLC-0 complex recorded at the times indicated in the figure. The configuration of the complex observed during the simulation varies to attain any of the configurations described in Figure 4D−F.

A common, most probable conformation for each ligand is observed during the MD, independent of the starting docking model.

Figure 6 presents an example of the movements observed in CPA at its binding site in CLC-0 during a MD simulation. The simulation was started from conformation II, and the initial configuration obtained after equilibration is indicated as $t = 0$. In this position, the distance between the carboxylic carbon of CPA and R312:CZ is about 10 Å. This distance reduces rapidly to less than 5 Å (see 45 ps) as CPA goes out from the pore. This approach is seen as a transient parallel increase of distance between the Cl^- ion inside the channel and the two extremes of the CPA molecule, the carboxyl carbon and Cl. After a few tens of picoseconds, CPA tends to assume the "parallel" conformation, where CPA is roughly parallel to helix **J** (see 75 ps), with the carboxy terminal closely interacting with the amino of R312 (in helix **J**), and the aromatic ring is near the hydrophobic surface of the helix **R** (L521 and P522). Some transitions to a position similar to conformation III, which occur by a rotation of CPA anchored by that interaction of the CPA's carboxyl group and R312, are observed (see 700 ps). In a MD simulation where the starting structure was conformation III, a transition to the parallel conformation was observed (data not shown). The characteristic feature in the most frequent conformation, parallel, of CPA in the CLC-0 pore is a close interaction of the ligand with the basic residues R302 and R312 and with P522.

*Effect of Mutations in Helices **J** and **R** on CPA Affinity.* To test the predictions of the geometrical docking results, we introduced mutations in the amino acids that are putatively interacting with CPA. The mutations were introduced in the WT CLC-0 construct containing the C212S mutation, which abolishes almost completely the gating transitions of the common pore gate (*31*), to avoid as much as possible of the interference of CPA block with the slow gate. Mutations included R305Q, R305E, and R312Q in helix **J** and P522S in helix **R** (see Figure 3B).

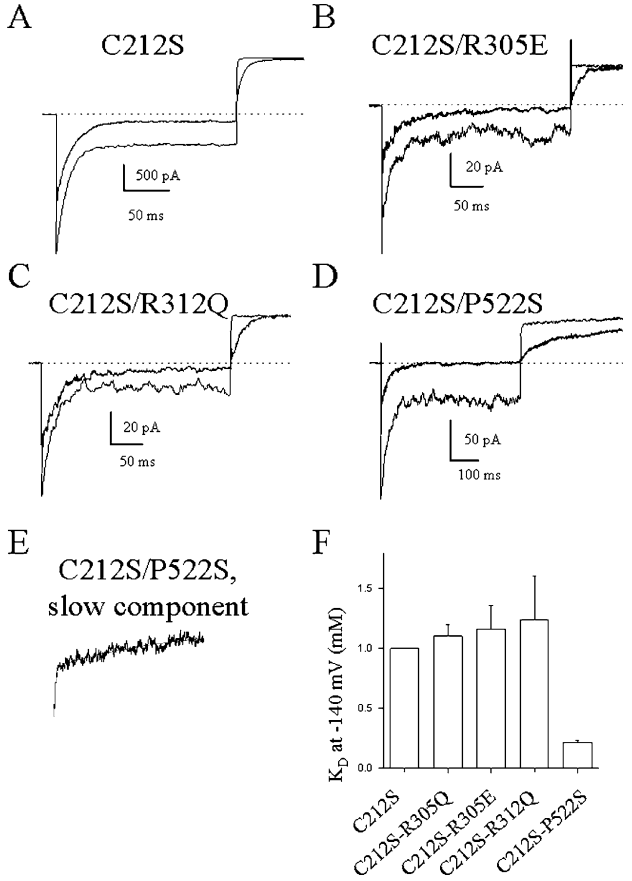

FIGURE 7: Representative current traces and apparent CPA affinity for mutants. (A−D) Current traces from the indicated mutants measured from inside-out patch without (thin black traces) and in the presence of 5 mM CPA (thick gray traces). The currents were evoked by the following pulse protocol: from a holding potential of 0 mV, a pulse was applied to −140 mV, followed by a pulse to +60 mV. Dotted lines indicate zero current. (E) Slow activation of mutant C212S/P522S at +60 mV (without CPA) taken from trace D is shown enlarged, superimposed with a double-exponential fit (gray trace) with the two time constants $\tau_f = 2.5$ ms and $\tau_s = 290$ ms. (F) Average apparent K_D for the steady-state inhibition at −140 mV is shown for the various mutants (±SEM, $n \geq 3$). For the C212S mutant, the value reported in ref *38* was taken.

In Figure 7 are shown the currents of C212S (A), C212S/R305E (B), C212S/R312Q (C), and C212S/P522S (D) in the absence (black traces) and in the presence of 5 mM CPA (gray traces). Currents of mutant C212S/R305Q are virtually identical to those of mutant C212S/R305E (data not shown). Without CPA, mutations of the arginines in helix **J** (positions 305 and 312) have practically the same voltage dependence and kinetics as the single mutation C212S. Currents deactivate normally at −140 mV within tens of milliseconds and activate rapidly and completely within about 1 ms at +60 mV. In contrast, mutant C212S/P522S exhibits subtle but important kinetic differences. In particular, gating relaxations have a double-exponential time course. For example, a slow component with a time constant of hundreds of milliseconds is visible at +60 mV (Figure 7E). On the basis of a more detailed analysis, we assume that the mutation P522S reintroduces transitions of the slow common pore gate (data not shown). Adding 5 mM CPA leads, in all cases, to a relatively strong block at −140 mV. At +60 mV, currents of the single C212S mutation and of the mutations in helix **J** are almost unaffected at steady state, while mutant C212S/P522S displays a reduction of about 40%.

From similar data obtained with 0.1, 1, 5, and 20 mM CPA, we estimated the apparent dissociation constant (K_D) at −140 mV at steady state (Figure 7F). While mutants in helix **J** were indistinguishable from the single mutation C212S, mutation C212S/P522S in helix **R** has an about 5-fold larger affinity than C212S. However, as it appears that the P522S mutation reintroduces at least partially the slow gate, it is unclear, at this point, if the increase in affinity is an indirect effect or if it reflects a direct interaction of the amino acid at position 522 with CPA.

Forced Molecular Dynamics. As the experimental results described above are not fully compatible with the positions of CPA found by the geometrical docking procedure, we applied a constant force to the CPA ligands in 7 independent simulations, starting from a random assignment of velocities. Each forced MD simulation was preceded by a 250-ps equilibration before application of the force on the CPA molecule located near the intracellular entrance of the pore of each subunit, pushing it toward its putative selectivity filter. We considered the data obtained on each subunit as an independent simulation, as the distance between the intracellular pores is larger than 40 Å. Since the cutoff of the energy calculation of nonbounded interactions was 12 Å, it is very unlikely that the events that we are monitoring on one subunit would influence significantly the other one.

From the actual 14 cases studied here, we discarded one from the analysis, as the CPA ligand did not follow the expected pathway toward the center of the ion pore. In this case, when a force of 483 fN (0.7 kcal mol^{-1} $Å^{-1}$) was applied to CPA, the ligand completely crossed the membrane, passing through the interface between the protein and the lipid bilayer. Although this kind of phenomenon is beyond the objective of this work, it is interesting to mention, as it could reveal a potential pathway for CPA to reach its target when applied to the extracellular side.

Figures 8 and 9 describe the complete process that we observed in most forced MD simulations. In these simulations, the CPA molecule was located near the entrance of the pore, and after equilibration, we applied a force of 138 fN (0.2 kcal mol^{-1} $Å^{-1}$). To monitor the position of the molecule during the dynamics, we measured the distance between the chlorine and the carboxylic carbon of CPA and several atoms of the protein. In Figure 8, we report the distances between the CPA atoms and NZ of K519, CD of E166, and OG1 of T471 for this simulation. As soon as the force was applied at the end of equilibration, CPA rapidly (less than 20 fs) moved to a position closer to the entrance of the pore and stayed there for the first 250 ns of the simulation, with a fluctuation less than 1 Å (Figure 9A). We defined the mean position of CPA in this configuration as "initial". The *initial* configuration of CPA is similar to the *parallel* configuration, which is the position found most frequently in MD simulations without any force applied (Figure 6B,C). The CPA in the *initial* configuration exerts a close interaction with the C-terminal of helices **J** and **R**, which define the intracellular entrance of the channel. As the simulation proceeds, a sudden change of orientation occurs at about 260 ns, when the longer CPA molecule axis (chlorine−carboxylic carbon) aligns with the axis of the channel and penetrates the pore. The orientation of the CPA molecule, with the carboxylic carbons pointing to the interior of the pore, was similar for all the simulations where the

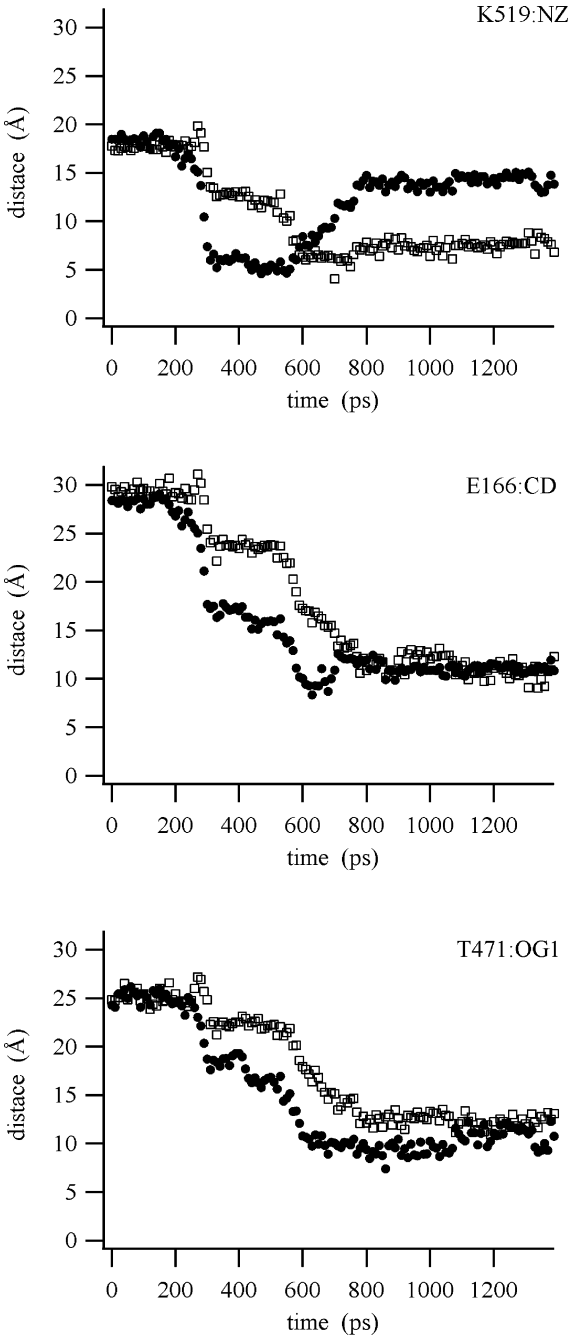

FIGURE 8: Trajectory of CPA and selected atoms of CLC-0 during a "forced" MD simulation. The distance between the chlorine (empty squares) and the carboxylic carbon (filled circles) of CPA and the CLC-0 atoms NZ of K519, CD of E166, and OG1 of T471 are plotted against the reference axis, defined by the vector of the applied force. A force of 138 fN was applied on CPA during the simulation. Snapshots of this simulations are shown in Figure 9.

ligand entered into the pore (12 of 13). In some cases, this "aligned" configuration is very similar to the configurations we obtained by geometrical docking (Figure 4D), with CPA in close contact with the **J**- and **H**-helix surfaces facing toward the pore and with the N-terminal of the **D**- and **N**-helices that form part of the pore region that coordinates the Cl^- ion inside the channel (*2*). In other simulations, such as that described in Figures 8 and 9, CPA in the *aligned* configuration is deeper in the pore, as shown in Figure 9B, decreasing its contact with **J**. In 7 of 13 simulations, CPA reaches a deeper position after a new transition (Figure 9C). In the *deep* configuration, CPA approaches closer to the **D**- and **N**-helices, but still maintains an interaction with the **J**- and **H**-helices. A second *deep* configuration (Figure 9D), where CPA rotates, approaching the **M**/**N** loop, was observed in 5 simulations.

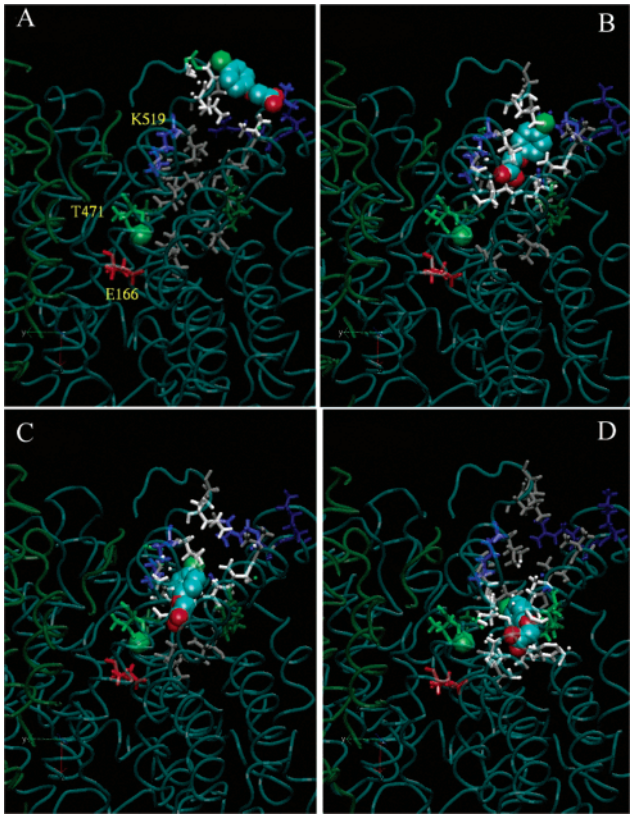

FIGURE 9: Snapshot of a "forced" MD of the CPA−CLC-0 complex's *initial* configuration recorded at 160 ps (A), the *aligned* configuration at 460 ps (B), and the two *deep* configurations recorded at 610 ps (C) and 1010 ps (D). The images of the figure correspond to the same simulation described in the trajectory presented in Figure 8. The CPA and Cl^- are represented in space-filling. Reference residues used for distance measurements in Figure 8 are indicated in part A.

Table 1 shows a summary of the results obtained from 13 forced 1.4-ns MD simulations with different applied forces. In 6 control MD simulations run in the same conditions, except that no force was applied, CPA neither approached the channel entrance nor attained any of the configurations inside the CLC-0 pore in 1.4 ns (data not shown). As expected, there is a tendency for CPA to reach a deeper configuration in the CLC-0 pore as the magnitude of the applied force is increased. We have not observed any further displacement of CPA when it reaches the final *deep* configuration (Figure 9C,D), even in 2 MD simulations continued for another 3 ns. In Table 1 are also indicated the specific residues that showed a close interaction with CPA in different configurations, as revealed by LIGPLOT. Notice that no hydrogen bonds were predicted by HHBOND in any CPA−CLC-0 configuration.

To characterize the forced MD simulations, we analyzed the time course of the displacement of CPA along a reference axis, defined by the applied force vector. Figure 10A shows the plot of the position of the baricenter of CPA in the reference axis as a function of time, as measured in same simulation described in Figures 8 and 9. The displacement plot shows a stepwise shape, as the CPA spends a given

Table 1: Summary of the "Forced" MD Simulations[a]

force (fN)	*initial*	*aligned*	*deep 1*	*deep 2*
69	4	3	1	1
138	4	4	2	1
207	2	2	1	0
345	2	2	2	2
483	1	1	1	1
total forced simulations	13	12	7	5
interactions	**J:** V309, K313 **R:** L521, P522	**D:** V121, G122 **J:** I308, R312 **M/N:** P412 **R:** I515, I518	**D:** V121, G122, S123 **J:** I308 **M/N:** P412, A417 **R:** I515, I518, K519	**D:** G122 **J:** N304 **M/N:** V409, T410, P412, A417, V421

[a] The number of simulations at which was found each CPA configurations indicated for each applied force. The two possible deep configurations are indicated separately. The specific interactions of CPA with CLC-0 residues yielded by the analysis with LIGPLOT are also presented. The helix and the residue identifications are presented.

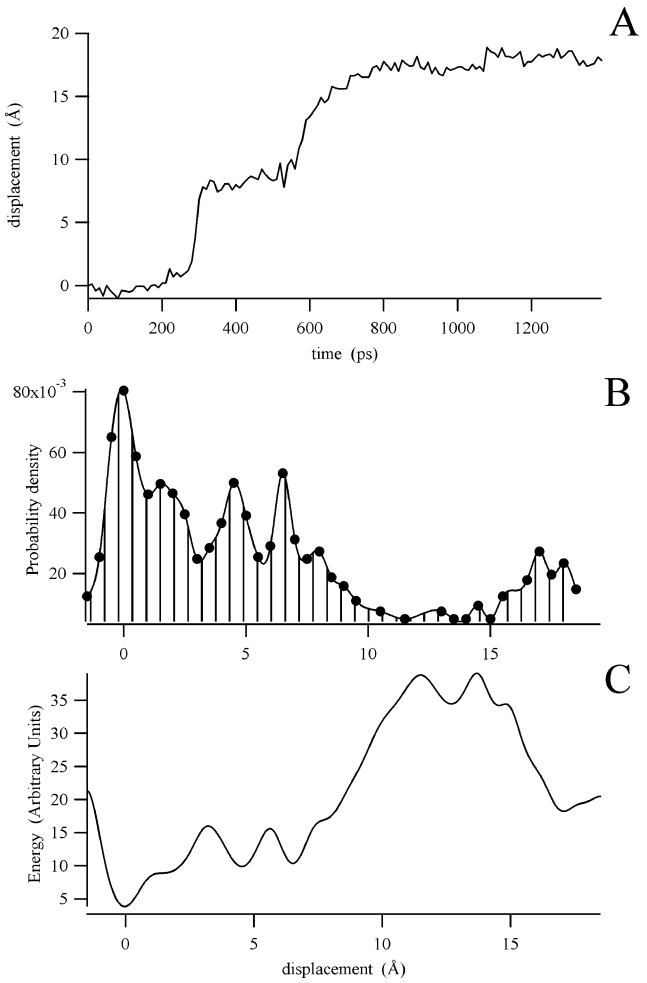

FIGURE 10: (A) Time course of the displacement of the baricenter of CPA along the axis of the applied force vector, measured during a "forced" MD of the CPA−CLC-0 complex. A force of 138 fN was applied on CPA during the simulation. (B) Overall probability density of the CPA displacement measured from 11 different simulations. The peaks, showing the positions with a higher probability of permanency of CPA into the CLC-0 pore, are the most probable binding sites. (C) Qualitative estimations of the energy profile of the CPA trajectory inside the channel. The energy, expressed in arbitrary units, was estimated as the negative logarithm of the probability measured in part B.

time on each configuration, before a relatively fast transition to the successive configuration. Three clearly distinct stationary levels shown in the plot correspond to *initial*, *aligned*, and *deep* configurations. As the transition between the two *deep* configurations does not require a significant displacement along the reference axis, these two configurations could not be resolved in the plot of Figure 10A.

From the time course of CPA trajectories along the reference axis obtained from all the forced MD simulations, we constructed the corresponding histograms of the CPA probability of remaining at a given position along the reference axis in a simulation. The overall probability histogram shown in Figure 10B was accumulated in a weighed sum (*28*) of 13 forced MD trajectories. The first peak corresponds to the *initial* configuration. The second and the third peaks, centered at 4.5 and 7.5 Å respectively, correspond to the *aligned* configurations in its two variants. Finally, the last peak, centered at 17.5 Å, corresponds to the *deep* configurations. These data allows us to propose a qualitative approximation to the energy profile of the CPA−CLC-0 channel pore along the reference axis. It can be obtained by estimating the energy E as proportional to the probability to stay on each position P_0, i.e., $E \propto -\ln(P_0)$, as shown in Figure 10C.

DISCUSSION

We have undertaken a study of the interaction of the small organic molecule CPA with the intracellular side of the CLC-0 channel pore. The work has four phases: (1) construction of a 3D model of the CLC-0 channel; (2) docking of the ligand to the intracellular pore mouth, to allow a guess of the binding site of CPA; (3) testing of the proposed model of binding by single-point mutation experiments; and (4) "forced" molecular dynamics simulation of the ligand−channel complex, to look for alternative configurations that fit better with experimental results.

The homology model of CLC-0 was restricted to helices from **B** to **R**, as those have a reasonable similarity with the bacterial StCLC channel and yield a reliable prediction. The structural model of CLC-0 obtained is probably the closed state of the channel, as suggested also for the bacterial channel (*2*). The feasibility of the CLC-0 model obtained was checked using well-established criteria (*21*, *22*, *36*, *37*), resulting in a set of parameters that indicates a moderately good quality of the simulation. The agreement of the CLC-0 model backbone to the StCLC structure, even after an intensive energy minimization procedure, is remarkably good (see Figure 2). This confirms that the general features of the StCLC channel may be applied to other CLC-family channels, constituting a good starting point for predictions

of the interaction of these channels with other molecules.

We used a blind geometrical approach to the toxin docking (*24*), which resulted in a set of 5000 geometrically acceptable conformations for the channel pore−toxin interaction, as expected for a system of two molecules with a high degree of freedom (three translations and three rotations). The first inspection of data, purely based on topological considerations, i.e., that the toxin must bind near the intracellular entrance of the channel, resulted in 15 conformations, which is still a high number of possible models. A closer inspection of these models demonstrated that, on the basis of their similarities, these configurations could be reduced to only three configurations (Figure 5).

As we had three possible binding configurations of CPA on the CLC-0 channels, we analyzed the MD trajectories to study the behavior of the ligand-to-receptor interactions. To avoid any boundary consideration on the MD, this study was done with the protein immersed in a phospholipid bilayer, and an appropriate water shell was created at the membrane surfaces (Figure 2E). The analysis of MD simulations of the CPA−CLC-0 complexes showed that the three sets of conformations are interconvertible, independent of the starting conformation, and there is a good possibility to find the other two conformations during a 2-ns MD simulation.

On the basis of the configurations proposed by the docking algorithm, we selected three amino acids of CLC-0 that are expected to interact strongly with CPA (R305 and R312 in helix **J**, and P522 in helix **R**) and investigated the effect of point mutations at these positions on the CPA block. While mutations in helix **J** had no effect on CPA inhibition, the P522S mutation slightly increased the apparent affinity. However, because the latter mutation also significantly altered the gating phenotype, it is quite possible that the effect is indirect. Thus, the conformations found by geometrical docking probably do not correspond to the final position of bound CPA but, at most, represent an intermediate configuration during the association process. Furthermore, the blockage of CLC-0 channels by CPA is strongly voltage-dependent. This is in contrast to a simple assumption of a binding site near the surface of the channel but strongly suggests that the CPA may enter into the ionic pathway. Second, preliminary data indicate that mutations on S123 and Y512, which lie deeper in the pore close to the Cl^- binding site, alter the affinity of CPA and its derivatives (*38*, *39*). Mutation of the glutamate putatively involved in the gating of the channel in CLC-1 (homologous to E166 in CLC-0), which removes the fast-gating mechanism of the channel, modifies the CPA affinity (*40*).

Hence, it is probably that CPA can actually arrive deeper in the pore, but the energy barrier to proceed toward its final position is too high to be overcome in the short simulation time (<4 ns). The obvious solution to this would be to extend the simulation to give time enough to attain a good probability to observe a transition between the external binding configuration and a hypothetical intrapore configuration. However, such long-time MD simulation protocols are unrealistic, as doing so for this system, which contains protein, lipids, and water (about 60 000 atoms), would be highly time-consuming. As an alternative, we decided to "force" the CPA to overcome the energy barriers by "pushing" it toward the center of the ion pathway by a constant force vector applied during the MD simulation. With this strategy, we were able to observe, in relatively short simulations (<1.5 ns), the CPA ligand overcoming the energy barriers and arriving at a plausible final binding position, near the putative gating mechanism of the channel. As a consequence, we can describe the binding of CPA to CLC-0 as a sequence of three successive binding sites. The CPA molecule in the *initial* configuration (Figure 9A) binds first to the intracellular position. Although the analysis of the mutation on P522 remains difficult to interpret, as it interferes with the slow gating mechanism per se, it is interesting to observe that this residue is in close contact with CPA in the *initial* conformation. Successively, the CPA moves to the *aligned* configuration, rotating to align its larger axis with that of the pore, with its carboxylic carbon toward the center of the channel (Figure 9B). Finally, in the last position, the *deep* configuration, CPA is in close contact with the N-terminal residues of **D**- and **N**- helices, which are putatively involved in the selectivity filter and/or the gating of the channel (*2*). The interaction of CPA in the *deep* configuration and the CLC channels may explain the anomalous gating modification produced by clofibric acid derivatives (*5*, *38*).

It has to be kept in mind that most data presented here have been obtained by simulation procedures. However, besides the strong limitations inherent to the study of models, the docking properties of the CPA, followed by traditional and "forced" molecular dynamic simulations, have provided a plausible hypothesis for ligand−channel interactions, and this opens the possibility to rationally design experiments to verify such a hypothesis.

REFERENCES

1. Jentsch, T. J., Stein, V., Weinreich, F., and Zdebik, A. A. (2002) *Physiol. Rev. 82*, 503−568.
2. Dutzler, R., Campbell, E. B., Cadene, M., Chait, B. T., and MacKinnon, R. (2002) *Nature 415*, 287−294.
3. Hille, B. (2001) *Ionic channels of excitable membranes*, Sinauer, Sunderland, MA.
4. Pusch, M., Liantonio, A., Bertorello, L., Accardi, A., De Luca, A., Pierno, S., Tortorella, V., and Conte Camerino, D. (2000) *Mol. Pharmacol. 58*, 498−507.
5. Pusch, M., Liantonio, A., Ferrera, L., De Luca, A., Conte Camerino, D., and Conti, F. (2001) *J. Gen. Physiol. 118*, 45−62.
6. Accardi, A., Ferrera, L., and Pusch, M. (2001) *J. Physiol. 534*, 745−752.
7. Lorenz, C., Pusch, M., and Jentsch, T. J. (1996) *Proc. Natl. Acad. Sci. U.S.A. 93*, 13362−13366.
8. Liantonio, A., Accardi, A., Carbonara, G., Fracchiolla, G., Loiodice, F., Tortorella, P., Traverso, S., Guida, P., Pierno, S., De Luca, A., Conte Camerino, D., and Pusch, M. (2002) *Mol. Pharmacol. 62*, 265−271.
9. Pusch, M., Accardi, A., Liantonio, A., Guida, P., Traverso, S., Conte-Camerino, D., and Conti, F. (2002) *Mol. Membr. Biol. 19*, 285−292.
10. De Luca, A., Tricarico, D., Wagner, R., Bryant, S. H., Tortorella, V., and Conte Camerino, D. (1992) *J. Pharmacol. Exp. Ther. 260*, 364−368.
11. Middleton, R. E., Pheasant, D. J., and Miller, C. (1996) *Nature 383*, 337−340.
12. Miller, C., and White, M. M. (1984) *Proc. Natl. Acad. Sci. U.S.A. 81*, 2772−2775.
13. Ludewig, U., Pusch, M., and Jentsch, T. J. (1996) *Nature 383*, 340−343.
14. Weinreich, F., and Jentsch, T. J. (2001) *J. Biol. Chem. 276*, 2347−2353.
15. Guex, N., and Peisch, M. C. (1997) *Electrophoresis 18*, 2717−2723.
16. Peisch, M. C. (1995) *Bio/Technology 13*, 658−660.
17. Peisch, M. C. (1996) *Biochem. Soc. Trans. 24*, 274−279.

18. Kalé, L., Skeel, R., Bhandarkar, M., Brunner, R., Attila Gursoy, A., Krawetz, N., Phillips, J., Shinozaki, A., Varadarajan, K., and Schulten, K. (1999) *J. Comput. Phys. 151*, 283−312.
19. Wang, J., Cieplak, P., and Kollman, P. A. (2000) *J. Comput. Chem. 21*, 1049−1074.
20. Case, D. A., Pearlman, D. A., Caldwell, J. W., Cheatham, T. E., III, Wang, J., Ross, W. S., Simmerling, C. L., Darden, T. A., Merz, K. M., Stanton, R. V., Cheng, A. L., Vincent, J. J., Crowley, M., Tsui, V., Gohlke, H., Radmer, R. J., Duan, Y., Pitera, J., Massova, I., Seibel, G. L., Singh, U. C., Weiner, P. K., and Kollman, P. A. (2002) *AMBER 7*, University of California, San Francisco.
21. Hooft, R. W. W., Vriend, G., Sander, C., and Abola, E. E. (1996) *Nature 381*, 272.
22. Vriend, G. (1990) *J. Mol. Graphics 8*, 52−56.
23. Casewit, C. J., Colwell, K. S., and Rappe, A. K. (1992) *J. Am. Chem. Soc. 114*, 10035−10046.
24. Katchalski-Katzir, E., Shariv, I., Eisenstein, M., Friesem, A. A., Aflalo, C., and Vakser, I. A. (1992) *Proc. Natl. Acad. Sci. U.S.A. 89*, 2195−2199.
25. Aiello, M., Moran, O., Pisciotta, M., and Gambale, F. (1998) *Eur. Biophys. J. 27*, 211−218.
26. Jorgensen, W. L., Chandrasekhar, J., Madura, J., Impey, R. W., and Klein, M. L. (1983) *J. Chem. Phys. 79*, 926−935.
27. Ryckaert, J., Bellemans, A., Ciccotti, G., and Paolini, G. V. (1988) *Phys. Rev. Lett. 60*, 128−131.
28. Gullinsgrud, J. R., Braun, R., and Schulten, K. (1999) *J. Comput. Phys. 151*, 190−211.
29. Wallace, A. C., Laskowski, R. A., and Thornton, J. M. (1995) *Protein Eng. 8*, 27−134.
30. McDonald, I. K., and Thornton, J. M. (1994) *J. Mol. Biol. 238*, 777−793.
31. Lin, Y. W., Lin, C. W., and Chen, T. Y. (1999) *J. Gen. Physiol. 114*, 1−12.
32. Hamill, O., Marty, A., Neher, E., Sakmann, B., and Sigworth, F. (1981) *Pflüg. Arch. 391*, 85−100.
33. Rhodes, G. (2000) *Crystalography: Make crystals clear*, Academic Press, London.
34. Ludewig, U., Pusch, M., and Jentsch, T. J. (1997) *Biophys. J. 73*, 789−797.
35. Ludewig, U., Jentsch, T. J., and Pusch, M. (1997) *J. Physiol. 498*, 691−702.
36. Morris, A. L., MacArthur, M. W., Hutchinson, E. G., and Thornton, J. M. (1992) *Proteins 12*, 345−364.
37. Laskowski, R. A., MacArthur, M. W., Moss, D. S., and Thornton, J. M. (1993) *J. Appl. Crystallogr. 26*, 283−291.
38. Accardi, A., Traverso, S., and Pusch, M. (2002) *Biophys. J. 82*, 13a.
39. Accardi, A. (2002) Gating and block of CLC type chloride. Tesi di Dottorato di Ricerca XIII Ciclo, Fisica. Università degli studi di Genova, Genoa.
40. Estevez, R., Schroeder, B. C., Accardi, A., Jentsch, T. J., and Pusch, M. (2003) *Neuron*, in press.
41. Varshney, A., Brooks, F. P., Jr., and Wright, W. P. (1994) *IEEE Computer Graph. Appl. 14*, 19−25.

BI027368O